Philipp Junker and Klaus Hackl*

A condensed variational model for thermo-mechanically coupled phase transformations in polycrystalline shape memory alloys

Abstract: We derive an energy-based material model for thermomechanically coupled phase transformations in polycrystalline shape memory alloys. For the variational formulation of the model, we use the principle of the minimum of the dissipation potential for nonisothermal processes for which only a minimal number of constitutive assumptions has to be made. By introducing a condensed formulation for the representative orientation distribution function, the resulting material model is numerically highly efficient. For a first analysis, we present the results of material point calculations, where the evolution of temperature as well as its influence on the mechanical material response is investigated.

Keywords: Orientation Distribution Function; Shape Memory Alloys; Thermal Coupling; Thermodynamic Extremum Principle; Variational Principle.

***Corresponding author: Klaus Hackl,** Lehrstuhl für Mechanik-Materialtheorie, Ruhr-Universität Bochum, Bochum, Germany, e-mail: klaus.hackl@rub.de
Philipp Junker: Lehrstuhl für Mechanik-Materialtheorie, Ruhr-Universität Bochum, Bochum, Germany

1 Introduction

Shape memory alloys are materials that possess the highly symmetric austenitic crystal lattice at high temperatures and a composition of martensitic variants of lower symmetry at low temperatures. This can be observed for other alloys, too. However, the unique property of shape memory alloys, which characterizes this class of materials, is that the transformation strain is nearly volume preserving. As a consequence, it is possible to induce the phase transformation from austenite to martensite and vice versa or from one martensitic configuration to another by mechanical loads because they are not inhibited by volumetric eigenstresses. Dependent on the current room temperature and thus the virgin crystallographic state, shape memory alloys can show the effect of pseudoelasticity or pseudoplasticity, which are both accompanied by plateaus in the stress-strain diagrams. For more details, we refer, for example, to [1].

At high temperatures, austenite is the prevalent phase. A previous stress-induced phase transformation from austenite to a certain composition of martensitic variants results again in the austenitic configuration when the external load is removed. Hence, this material behavior is called pseudoelastic.

At low temperatures, where a uniform distribution of martensites forms the initial crystallographic state, an external mechanical load forces the material to accommodate its internal microstructure via detwinning. This means that some martensitic variants, which have a more favorable orientation than others, grow at the expense of the remaining ones. Because a martensitic crystal lattice has only low symmetry, it is easy to imagine that the initial configuration of uniformly distributed martensite cannot be recovered when the external load is removed. Hence, the material relaxes elastically, but a remaining deformation indicates a deviation from a state with uniformly distributed martensitic variants. If such a specimen is heated, thermally induced phase transformation takes place from the specific martensitic configuration to the austenitic one. Subsequent cooling restores the initial state of undeformed uniformly distributed martensite. Therefore, the observed material behavior is termed pseudoplastic. The described so-called one-way effect gives rise to the notion “shape memory alloys.”

Various experiments, for example in [2], show that, due to the dissipative character of phase transitions, which can be identified by the hysteresis observed in stress-strain diagrams, mechanical energy is partly converted into heat. The resultant change in temperature, on the contrary, has a direct consequence for the phase transformations: because a higher temperature stabilizes the austenite, phase transformation is slowed down if temperature is increased. This implies that the hysteresis in the stress-strain diagram increases its slope the higher the temperature is. This effect is more pronounced if more energy is converted into heat [2].

In this paper, we present a material model for the simulation of polycrystalline shape memory alloys, which accounts for thermal coupling. The model uses a novel

approach involving a condensed orientation distribution function. This one is based on representing the entire texture of the polycrystalline aggregate by its average orientation. This way, the number of degrees of freedom is reduced drastically and the numerical effort by orders of magnitude compared with previous works. We use the variational concept of the minimum of the dissipation potential for nonisothermal processes, as presented in [3], which allows to derive a thermomechanically coupled material model. Additionally, this approach results in a more concise mathematical structure of the equations compared with the principle of maximum dissipation [3]. A variational or energy-based material model has the advantage that it must be calibrated only once. Afterwards, results of comparable quality can be obtained for different load states and geometries at different temperatures. This concept is expanded in this paper by the thermomechanically coupled version of the material model.

This work is based on a model in [4, 5], which has been investigated within a finite element scheme in [6]. A thermomechanically coupled version of this model, based on the principle of maximum dissipation, was presented in [7, 8]. Previous models for shape memory alloys based on phenomenological concepts can be found, for instance, in [9–11]. A selection of other micromechanical models is derived in [12–14].

2 Material model

The principle of the minimum of the dissipation potential for nonisothermal processes states that

$$\mathscr{L} = \overline{\mathscr{D}} - \mathscr{D} \rightarrow \min_{\dot{\xi}, \mathbf{q}} \tag{1}$$

see [3]. In Equation (1), $\dot{\xi}$ are the rates of the internal variables of the specific material model, $\mathbf{q}$ is the heat flux vector, and $\mathscr{D}$ is the thermodynamic dissipation, which is given by the second law of thermodynamics. This is

$$\mathscr{D} = -\dot{\psi} - \frac{1}{\theta}\mathbf{q}\cdot\nabla\theta, \tag{2}$$

with the Helmholtz free energy ψ and the (absolute) temperature θ. We introduce two kinds of internal variables, namely, a vector of volume fractions of the crystallographic phases denoted by $\boldsymbol{\lambda}=(\lambda_i)$, λ_0 representing the austenite and λ_i, $i\in\{1, \ldots, \overline{n}\}$ representing the specific martensitic variants, where $\overline{n}$ is alloy dependent, and a set of three Euler angles $\boldsymbol{\alpha}$, which indicates the average or mean orientation direction of the polycrystalline arrangement.

Thus, the rate of the internal variables is $\dot{\xi}=\{\dot{\boldsymbol{\lambda}}, \dot{\boldsymbol{\alpha}}\}$. We denote by $\overline{\mathscr{D}}$ the so-called dissipation potential introduced in [15] comprising the material-dependent dissipative terms. We decompose the dissipation potential into a transformational and a thermal part as $\overline{\mathscr{D}}=\overline{\mathscr{D}}^{\mathrm{tr}}+\overline{\mathscr{D}}^{\mathrm{th}}$. Moreover, we set $\overline{\mathscr{D}}^{\mathrm{tr}}=r_\lambda|\dot{\boldsymbol{\lambda}}|+r_\alpha|\dot{\boldsymbol{\alpha}}|$ and follow [3] to set $\overline{\mathscr{D}}^{\mathrm{th}}=\mu|\mathbf{q}|^2/(2\theta)$, where r_λ and r_α are the dissipation parameters for phase transformation and reorientation, respectively, and μ is the reciprocal of the heat conductivity [3].

The Lagrangean $\mathscr{L}$ in Equation (1) is not minimized with respect to the rates of the strains. Hence, we drop the term $(\partial\psi/\partial\epsilon)\colon\dot{\epsilon}$ and find

$$\begin{aligned}\mathscr{L} = {} & r_\lambda|\dot{\boldsymbol{\lambda}}| + r_\alpha|\dot{\boldsymbol{\alpha}}| + \frac{\mu}{2\theta}|\mathbf{q}|^2 + \frac{\partial\psi}{\partial\boldsymbol{\lambda}}\cdot\dot{\boldsymbol{\lambda}} + \frac{\partial\psi}{\partial\boldsymbol{\alpha}}\cdot\dot{\boldsymbol{\alpha}} + \frac{1}{\theta}\mathbf{q}\cdot\nabla\theta \\ & -\boldsymbol{\gamma}\cdot\dot{\boldsymbol{\lambda}} + \beta\sum_{i=0}^{\overline{n}}\dot{\lambda}_i \rightarrow \min_{\dot{\boldsymbol{\lambda}}, \dot{\boldsymbol{\alpha}}, \mathbf{q}}\end{aligned} \tag{3}$$

The last two terms in Equation (3), $-\boldsymbol{\gamma}\cdot\dot{\boldsymbol{\lambda}}$ and $\beta\sum_{i=0}^{\overline{n}}\dot{\lambda}_i$, are introduced to include the constraints of positivity and mass conservation, respectively, by means of the Lagrange parameter β and the Kuhn-Tucker parameters $\boldsymbol{\gamma}=(\gamma_i)$. For more details, we refer to [4, 5].

The stationarity condition of $\mathscr{L}$ with respect to the rates of the volume fractions reads, due to the nondifferentiability of $|\dot{\boldsymbol{\lambda}}|$ at $\dot{\boldsymbol{\lambda}}=\mathbf{0}$, the differential inclusion

$$r_\lambda\frac{\dot{\boldsymbol{\lambda}}}{|\dot{\boldsymbol{\lambda}}|} + \frac{\partial\psi}{\partial\boldsymbol{\lambda}} - \boldsymbol{\gamma} + \boldsymbol{\beta} \ni \mathbf{0}, \tag{4}$$

where $\boldsymbol{\beta}=\beta\mathbf{1}$ and $\mathbf{1}$ denotes the $\overline{n}+1$-dimensional vector with value 1 in all components. The stationarity condition of $\mathscr{L}$ with respect to the rates of the Euler angles gives

$$r_\alpha\frac{\dot{\boldsymbol{\alpha}}}{|\dot{\boldsymbol{\alpha}}|} + \frac{\partial\psi}{\partial\boldsymbol{\alpha}} \ni \mathbf{0}. \tag{5}$$

Finally, stationarity of $\mathscr{L}$ with respect to $\mathbf{q}$ yields

$$\mathbf{q} = -\frac{1}{\mu}\nabla\theta \tag{6}$$

which is nothing else but Fourier's law of heat conduction.

It turns out to be convenient to invert Equations (4) and (5), which amounts to performing a Legendre transformation of the dissipation potentials $\overline{\mathscr{D}}^{\mathrm{tr}}$ and $\overline{\mathscr{D}}^{\mathrm{th}}$. For this purpose, let us introduce an active set (of variants) $\mathscr{A}$ as

$$\mathscr{A} = \{i\,|\,\lambda_i\neq 0\}\cup\{i\,|\,\lambda_i = 0\wedge\dot{\lambda}_i > 0\} \tag{7}$$

to account for the constraint of positivity and furthermore $\mathbf{p}^\lambda=-\partial\psi/\partial\boldsymbol{\lambda}$ and $\mathbf{p}^\alpha=-\partial\psi/\partial\boldsymbol{\alpha}$ as thermodynamically

conjugated driving forces. Inserting this into Equation (4), we find

$$\begin{cases} p_i^\lambda - \dfrac{1}{\bar{n}_{\mathscr{A}}} \sum\limits_{k\in\mathscr{A}} p_k^\lambda = r_\lambda \dfrac{\dot{\lambda}_i}{|\dot{\boldsymbol{\lambda}}|}, & i\in\mathscr{A}, \\ p_i^\lambda - \dfrac{1}{\bar{n}_{\mathscr{A}}} \sum\limits_{k\in\mathscr{A}} p_k^\lambda = -\gamma_i < 0, & i\in\mathscr{A}. \end{cases} \tag{8}$$

Following [4, 5], we introduce the active deviator as

$$\mathrm{dev}_{\mathscr{A}}\, \mathbf{p}^\lambda := \mathbf{p}^\lambda - \frac{1}{\bar{n}_{\mathscr{A}}} \sum_{k\in\mathscr{A}} p_k^\lambda \mathbf{1} \tag{9}$$

with $\bar{n}_{\mathscr{A}}$ as number of active phases. This allows to define yield functions $\Phi_\lambda \le 0$ and $\Phi_\alpha \le 0$, which indicate whether phase transformation and/or reorientation take place, respectively. They are given as

$$\Phi_\lambda = |\mathrm{dev}_{\mathscr{A}}\, \mathbf{p}^\lambda|^2_{\mathscr{A}} - r_\lambda^2. \tag{10}$$

and

$$\Phi_\alpha = \mathbf{p}^\alpha \cdot \mathbf{p}^\alpha - r_\alpha^2, \tag{11}$$

where $|\mathbf{p}|^2_{\mathscr{A}} = \sum_{i\in\mathscr{A}} p_i^2$. We take the formula given in [3] to derive the heat conduction equation. Using our approach for $\overline{\mathscr{D}}^{\mathrm{th}}$, it is given as

$$\kappa\dot{\theta} - \nabla\cdot\left(\frac{1}{\mu}\nabla\theta\right) = \mathbf{p}^\lambda\cdot\dot{\boldsymbol{\lambda}} + \mathbf{p}^\alpha\cdot\dot{\boldsymbol{\alpha}} + \dot{p}_\theta\theta, \tag{12}$$

where κ denotes the heat capacity. Structural heating $\dot{p}_\theta\theta$ is defined via

$$p_\theta = -\frac{\partial\psi}{\partial\theta}. \tag{13}$$

For the Helmholtz free energy, we take the approach from [4, 5], now including temperature-dependent parts, as

$$\psi = \frac{1}{2}(\boldsymbol{\epsilon} - \mathbf{Q}^{\mathrm{T}}\cdot\bar{\boldsymbol{\eta}}\cdot\mathbf{Q}) : \bar{\mathbb{C}} : (\boldsymbol{\epsilon} - \mathbf{Q}^{\mathrm{T}}\cdot\bar{\boldsymbol{\eta}}\cdot\mathbf{Q}) + \bar{c}(\theta), \tag{14}$$

where $\mathbf{Q}=\mathbf{Q}(\boldsymbol{\alpha})$ denotes a rotation matrix, and the effective transformation strain $\bar{\boldsymbol{\eta}}$, the effective stiffness tensor $\bar{\mathbb{C}}$, and the effective caloric part of the energy $\bar{c}(\theta)$ are given by

$$\bar{\boldsymbol{\eta}} = \sum_{i=0}^{\bar{n}} \lambda_i \boldsymbol{\eta}_i, \quad \bar{\mathbb{C}} = \left[\sum_{i=0}^{\bar{n}} \lambda_i (\mathbb{C}_i)^{-1}\right]^{-1}, \quad \bar{c}(\theta) = \sum_{i=0}^{\bar{n}} \lambda_i c_i(\theta). \tag{15}$$

According to [16], the temperature-dependent caloric part of the energy is given as

$$c_i(\theta) = a_i - b_i\theta, \tag{16}$$

where we have omitted terms that are identical for all phases and therefore are not relevant for our formulation.

We are now able to write the final system of evolution equations as

$$\dot{\boldsymbol{\lambda}} = \rho_\lambda (\mathrm{dev}_{\mathscr{A}}\, \mathbf{p}^\lambda)_{\mathscr{A}}, \tag{17}$$

$$\dot{\boldsymbol{\alpha}} = \rho_\alpha \mathbf{p}^\alpha \tag{18}$$

with $\rho_\lambda := |\dot{\boldsymbol{\lambda}}|/r_\lambda$ and $\rho_\alpha := |\dot{\boldsymbol{\alpha}}|/r_\alpha$ as consistency parameters. The Kuhn-Tucker conditions

$$\rho_\lambda \ge 0, \qquad \Phi_\lambda \le 0, \qquad \rho_\lambda\Phi_\lambda = 0, \tag{19}$$

$$\rho_\alpha \ge 0, \qquad \Phi_\alpha \le 0, \qquad \rho_\alpha\Phi_\alpha = 0, \tag{20}$$

close the system of equations, in combination with the consistency condition

$$\mathrm{dev}_{\mathscr{A}}\, p_i^\lambda \le 0 \qquad \text{for } i\notin\mathscr{A} \tag{21}$$

which updates the active set. The heat conduction equation reads

$$\kappa\dot{\theta} - \nabla\cdot\left(\frac{1}{\mu}\nabla\theta\right) = \mathbf{p}^\lambda\cdot\dot{\boldsymbol{\lambda}} + \mathbf{p}^\alpha\cdot\dot{\boldsymbol{\alpha}} - \mathbf{b}\cdot\dot{\boldsymbol{\lambda}}\theta \tag{22}$$

with $\mathbf{b}=(b_{\mathrm{A}}, b_{\mathrm{M}}, \ldots, b_{\mathrm{M}})$, where b_{A} and b_{M} denote the entropic constants for austenite and martensite, respectively.

To evaluate the material model, it is necessary to derive the driving forces. For the volume fractions, they are

$$\begin{aligned} p_i^\lambda = {} & (\mathbf{Q}^T\cdot\boldsymbol{\eta}_i\cdot\mathbf{Q}) : \bar{\mathbb{C}} : (\varepsilon - \mathbf{Q}^T\cdot\bar{\boldsymbol{\eta}}\cdot\mathbf{Q}) \\ & + \frac{1}{2}(\varepsilon - \mathbf{Q}^T\cdot\bar{\boldsymbol{\eta}}\cdot\mathbf{Q}) : [\bar{\mathbb{C}} : (\mathbb{C}_i)^{-1} : \bar{\mathbb{C}}] : (\varepsilon - \mathbf{Q}^T\cdot\bar{\boldsymbol{\eta}}\cdot\mathbf{Q}) - \mathrm{c}_i(\theta). \end{aligned} \tag{23}$$

see also [4, 5]. The rotation matrix is given in terms of Euler angles as

$$\mathbf{Q}(\boldsymbol{\alpha}) = \begin{pmatrix} \cos\varphi\,\cos\omega - \cos\nu\,\sin\varphi\,\sin\omega & -\cos\nu\,\cos\omega\,\sin\varphi - \cos\varphi\,\sin\omega & \sin\nu\,\sin\varphi \\ \cos\omega\,\sin\varphi + \cos\nu\,\cos\varphi\,\sin\omega & \cos\nu\,\cos\varphi\,\cos\omega - \sin\varphi\,\sin\omega & -\cos\varphi\,\sin\nu \\ \sin\nu\,\sin\omega & \cos\omega\,\sin\nu & \cos\nu \end{pmatrix} \tag{24}$$

with $\boldsymbol{\alpha}=\{\varphi, \nu, \omega\}$ and $\varphi, \omega \in [0, 2\pi]$, $\nu \in [0, \pi]$. Now, we can calculate the corresponding driving forces as

$$\mathbf{p}^{\alpha} = -\frac{\partial \psi}{\partial \boldsymbol{\alpha}} = -\frac{\partial \psi}{\partial \mathbf{Q}} : \frac{\partial \mathbf{Q}}{\partial \boldsymbol{\alpha}} \tag{25}$$

Whereas the first term in Equation (25) reads

$$-\frac{\partial \psi}{\partial \mathbf{Q}} = 2[\overline{\boldsymbol{\eta}} \cdot \mathbf{Q} \cdot \overline{\mathbb{C}} : (\varepsilon - \mathbf{Q}^{T} \cdot \overline{\boldsymbol{\eta}} \cdot \mathbf{Q})], \tag{26}$$

the entries of the second part $\partial\mathbf{Q}/\partial\boldsymbol{\alpha}=(\partial\mathbf{Q}/\partial\varphi,\ \partial\mathbf{Q}/\partial\nu,\ \partial\mathbf{Q}/\partial\omega)$ are

$$\frac{\partial \mathbf{Q}}{\partial \varphi} = \begin{pmatrix} -\cos\omega\ \sin\varphi - \cos\nu\ \cos\varphi\ \sin\omega & -\cos\nu\ \cos\omega\ \cos\omega + \sin\varphi\ \sin\omega & \cos\varphi\ \sin\nu \\ \cos\varphi\ \cos\omega - \cos\nu\ \sin\varphi\ \sin\omega & -\cos\nu\ \cos\varphi\ \sin\varphi - \cos\varphi\ \sin\omega & \sin\nu\ \cos\varphi \\ 0 & 0 & 0 \end{pmatrix} \tag{27}$$

$$\frac{\partial \mathbf{Q}}{\partial \nu} = \begin{pmatrix} \sin\nu\ \sin\varphi\ \sin\omega & \cos\omega\ \sin\nu\ \sin\varphi & \cos\nu\ \sin\varphi \\ -\cos\varphi\ \sin\nu\ \sin\omega & -\cos\varphi\ \cos\omega\ \sin\nu & -\cos\nu\ \cos\varphi \\ \cos\nu\ \sin\omega & \cos\nu\ \cos\omega & -\sin\nu \end{pmatrix}, \tag{28}$$

$$\frac{\partial \mathbf{Q}}{\partial \omega} = \begin{pmatrix} -\cos\nu\ \cos\omega\ \sin\varphi - \cos\varphi\ \sin\omega & -\cos\varphi\ \cos\omega + \cos\nu\ \sin\varphi\ \sin\omega & 0 \\ \cos\nu\ \cos\varphi\ \cos\omega - \sin\varphi\ \sin\omega & -\cos\omega\ \sin\varphi - \cos\nu\ \cos\varphi\ \sin\omega & 0 \\ \cos\omega\ \sin\nu & -\sin\nu\ \sin\omega & 0 \end{pmatrix}, \tag{29}$$

3 Material point analysis

The evolution equations for the volume fractions and the Euler angles, Equations (19) and (20), can be evaluated if the strain is known as a function of time. Hence, for our purpose of analyzing the material point behavior of the model, no modifications are necessary. In contrast, the temperature gradient in Equation (22) cannot be evaluated at a material point level. There are several possibilities to reduce the equation in an appropriate way. One would be to consider the isothermal case, where all heat is immediately transported away when produced. Obviously, this case is of minor interest because it ignores thermal coupling completely. Therefore, we choose to investigate another possibility that is an adiabatic process. In such a system, no heat may enter or leave the system. Thus, for our case, all heat produced in the material point is converted directly into temperature changes. We find the material point heat conduction equation in its reduced form as

$$\kappa\dot{\theta} = \mathbf{p}^{\lambda} \cdot \dot{\boldsymbol{\lambda}} + \mathbf{p}^{\alpha} \cdot \dot{\boldsymbol{\alpha}} - \mathbf{b} \cdot \dot{\boldsymbol{\lambda}}\theta. \tag{30}$$

Due to its high nonlinearity, we solve the system of governing equations (17), (18), and (30) numerically.

On inspection of the equations, we find that our model is rate independent for a material point analysis, that is, the results do not change when altering the velocities of the process. Especially, for an adiabatic process, the loading velocity, defined as $\dot{\epsilon}$, has no influence on the heat production and thus temperature evolution. This means that we can replace the rates in Equation (30) by increments

$$\Delta\theta = \theta^{n+1} - \theta^{n}, \quad \Delta\boldsymbol{\lambda} = \boldsymbol{\lambda}^{n+1} - \boldsymbol{\lambda}^{n}, \quad \Delta\boldsymbol{\alpha} = \boldsymbol{\alpha}^{n+1} - \boldsymbol{\alpha}^{n}, \tag{31}$$

The unknown values of temperature, volume fractions, and Euler angles at the end of the time increment are indicated by $(\cdot)^{n+1}$, the known ones at the beginning by $(\cdot)^{n}$. On substitution, we obtain the time discretized form of the heat conduction equation. We are using a forward Euler scheme for the solution as

$$\kappa(\theta^{n+1} - \theta^{n}) = (\mathbf{p}^{\lambda})^{n} \cdot \Delta\boldsymbol{\lambda} + (\mathbf{p}^{\alpha})^{n} \cdot \Delta\boldsymbol{\alpha} - \mathbf{b} \cdot \Delta\boldsymbol{\lambda}\theta^{n+1} \tag{32}$$

from which the current temperature can be calculated as

$$\theta^{n+1} = \frac{\kappa\theta^{n} + (\mathbf{p}^{\lambda})^{n} \cdot \Delta\boldsymbol{\lambda} + (\mathbf{p}^{\alpha})^{n} \cdot \Delta\boldsymbol{\alpha}}{\kappa + \mathbf{b} \cdot \Delta\boldsymbol{\lambda}}. \tag{33}$$

The driving forces are evaluated using the known quantities at the beginning of the time increment. The discretized versions of Equations (17) and (18) then read

$$\Delta\boldsymbol{\lambda} = \hat{\rho}_{\lambda}(\operatorname{dev}_{\mathcal{A}}(\mathbf{p}^{\lambda})^{n})_{\mathcal{A}}, \qquad \Delta\boldsymbol{\alpha} = \hat{\rho}_{\alpha}(\mathbf{p}^{\alpha})^{n}. \tag{34}$$

The yield conditions are evaluated at the end of the time increment:

$$\Phi_{\lambda}(\boldsymbol{\lambda}^{n+1}, \boldsymbol{\alpha}^{n+1}) \le 0, \qquad \Phi_{\alpha}(\boldsymbol{\lambda}^{n+1}, \boldsymbol{\alpha}^{n+1}) \le 0 \tag{35}$$

The update of the variables is now calculated in a staggered scheme. In a first step, Equations (34) and (35),

together with the Kuhn-Tucker conditions, are solved for $\boldsymbol{\lambda}^{n+1}$, $\boldsymbol{\alpha}^{n+1}$, and the discretized consistency parameters $\hat{\rho}_\lambda, \hat{\rho}_\alpha$. In a second step, the temperature is updated according to Equation (33).

4 Numerical experiments

We apply our material model to nickel titanium, which can form 12 martensitic variants, yielding $\overline{n}=12$. The respective transformation strains for the different martensitic variants after [17] are collected in Table 1 ($\boldsymbol{\eta}_0=\mathbf{0}$). For the elastic constants of austenite and martensite, we use the expectation values, based on experimental data of [17] and [18], Table 2.

The values for the caloric part of the Helmholtz free energy, $\Delta c(\theta) := c_0(\theta) - c_1 > 0(\theta) = \Delta a - \Delta b\theta$, are chosen as $\Delta a = 0.258$ GPa and $\Delta b = 0.001$ GPa/K. The initial temperature is set to $\theta^0 = 323.15$ K, which implies $\Delta c(\theta^0) = -0.065$ GPa. The dissipation parameter for phase transformation is set to $r_\lambda = 0.013$ GPa.

The value for r_α controls the intensity of stress drop when phase transformation initializes and the plateau has not yet been completely established. Here, we choose it to be $r_\alpha = 0.001$ GPa.

The only remaining parameter is the heat capacity. As pointed out previously, on a material point level for the adiabatic case, the amount of produced heat is independent of the loading velocities. In other words, it is completely determined by the material parameters. Consequently, for demonstration of our material model, we vary the only parameter that is not fixed yet: the heat capacity κ. This allows to influence the magnitude of temperature change and therefore to investigate the material model for different cases. In a finite element setting, this modification is not necessary because then the temperature gradient in the heat conduction equation is still present and the dependence on the loading velocity is still given. However, for this first analysis, we present various sets of simulations with different values of the heat capacity, specifically $\kappa \in \{0.010, 0.015, 0.030, 0.050\}$ GPa/K. The larger the heat capacity is, the smaller the change in temperature. Hence, we expect higher temperatures for smaller heat capacity and therefore a larger influence on the mechanical material response compared with an isothermal case.

Table 1 Transformation strains for cubic to monoclinic transforming nickel titanium after [17].

$$\boldsymbol{\eta}_1 = \begin{pmatrix} \overline{\alpha} & \overline{\delta} & \overline{\epsilon} \\ \overline{\delta} & \overline{\alpha} & \overline{\epsilon} \\ \overline{\epsilon} & \overline{\epsilon} & \overline{\beta} \end{pmatrix} \quad \boldsymbol{\eta}_2 = \begin{pmatrix} \overline{\alpha} & \overline{\delta} & -\overline{\epsilon} \\ \overline{\delta} & \overline{\alpha} & -\overline{\epsilon} \\ -\overline{\epsilon} & -\overline{\epsilon} & \overline{\beta} \end{pmatrix} \quad \boldsymbol{\eta}_3 = \begin{pmatrix} \overline{\alpha} & -\overline{\delta} & -\overline{\epsilon} \\ -\overline{\delta} & \overline{\alpha} & \overline{\epsilon} \\ -\overline{\epsilon} & \overline{\epsilon} & \overline{\beta} \end{pmatrix}$$

$$\boldsymbol{\eta}_4 = \begin{pmatrix} \overline{\alpha} & -\overline{\delta} & \overline{\epsilon} \\ -\overline{\delta} & \overline{\alpha} & -\overline{\epsilon} \\ \overline{\epsilon} & -\overline{\epsilon} & \overline{\beta} \end{pmatrix} \quad \boldsymbol{\eta}_5 = \begin{pmatrix} \overline{\alpha} & \overline{\epsilon} & \overline{\delta} \\ \overline{\epsilon} & \overline{\beta} & \overline{\epsilon} \\ \overline{\delta} & \overline{\epsilon} & \overline{\alpha} \end{pmatrix} \quad \boldsymbol{\eta}_6 = \begin{pmatrix} \overline{\alpha} & -\overline{\epsilon} & \overline{\delta} \\ -\overline{\epsilon} & \overline{\beta} & -\overline{\epsilon} \\ \overline{\delta} & -\overline{\epsilon} & \overline{\alpha} \end{pmatrix}$$

$$\boldsymbol{\eta}_7 = \begin{pmatrix} \overline{\alpha} & -\overline{\epsilon} & -\overline{\delta} \\ -\overline{\epsilon} & \overline{\beta} & \overline{\epsilon} \\ -\overline{\delta} & \overline{\epsilon} & \overline{\alpha} \end{pmatrix} \quad \boldsymbol{\eta}_8 = \begin{pmatrix} \overline{\alpha} & \overline{\epsilon} & -\overline{\delta} \\ \overline{\epsilon} & \overline{\beta} & -\overline{\epsilon} \\ -\overline{\delta} & -\overline{\epsilon} & \overline{\alpha} \end{pmatrix} \quad \boldsymbol{\eta}_9 = \begin{pmatrix} \overline{\beta} & \overline{\epsilon} & \overline{\epsilon} \\ \overline{\epsilon} & \overline{\alpha} & \overline{\delta} \\ \overline{\epsilon} & \overline{\delta} & \overline{\alpha} \end{pmatrix}$$

$$\boldsymbol{\eta}_{10} = \begin{pmatrix} \overline{\beta} & -\overline{\epsilon} & -\overline{\epsilon} \\ -\overline{\epsilon} & \overline{\alpha} & \overline{\delta} \\ -\overline{\epsilon} & \overline{\delta} & \overline{\alpha} \end{pmatrix} \quad \boldsymbol{\eta}_{11} = \begin{pmatrix} \overline{\beta} & -\overline{\epsilon} & -\overline{\epsilon} \\ -\overline{\epsilon} & \overline{\alpha} & -\overline{\delta} \\ \overline{\epsilon} & -\overline{\delta} & \overline{\alpha} \end{pmatrix} \quad \boldsymbol{\eta}_{12} = \begin{pmatrix} \overline{\beta} & -\overline{\epsilon} & -\overline{\epsilon} \\ \overline{\epsilon} & \overline{\alpha} & -\overline{\delta} \\ -\overline{\epsilon} & -\overline{\delta} & \overline{\alpha} \end{pmatrix}$$

$\overline{\alpha}=0.02381$, $\overline{\beta}=-0.02480$, $\overline{\delta}=0.07528$, $\overline{\epsilon}=0.04969$.

Table 2 Expectation values for the elastic constants for austenite and martensite in NiTi, based on the experiments in [18] and [17].

$$\mathbb{C}_0 = \begin{pmatrix} 149.36 & 105.32 & 105.32 & 0 & 0 & 0 \\ 105.32 & 149.36 & 105.32 & 0 & 0 & 0 \\ 105.32 & 105.32 & 149.36 & 0 & 0 & 0 \\ 0 & 0 & 0 & 44.04 & 0 & 0 \\ 0 & 0 & 0 & 0 & 44.04 & 0 \\ 0 & 0 & 0 & 0 & 0 & 44.04 \end{pmatrix} \text{ GPa}$$

$$\mathbb{C}_{i>0} = \begin{pmatrix} 205.05 & 120.78 & 120.78 & 0 & 0 & 0 \\ 120.78 & 205.05 & 120.78 & 0 & 0 & 0 \\ 120.78 & 120.78 & 205.05 & 0 & 0 & 0 \\ 0 & 0 & 0 & 84.28 & 0 & 0 \\ 0 & 0 & 0 & 0 & 84.28 & 0 \\ 0 & 0 & 0 & 0 & 0 & 84.28 \end{pmatrix} \text{ GPa}$$

Strain is the input variable. We perform a numerical triaxial tension test for which we set

$$\epsilon = \chi \begin{pmatrix} 1 & 0 & 0 \\ 0 & -0.41 & 0 \\ 0 & 0 & -0.41 \end{pmatrix} \tag{36}$$

with $\chi \in [0, 0.06]$ linearly varying in time. The material is subjected to loading and unloading; consequently, χ increases linearly from zero to its maximum value and then decreases linearly again until it reaches zero. As randomly chosen initial set for the Euler angles, we take $\boldsymbol{\alpha}_0 = \{2.62596, 1.84057, 5.98139\}$ (rad).

At first, we show the evolution of temperature over strain in Figure 1. We see that, in the beginning, temperature is constant. At a strain of approximately $\chi = 0.0125$, phase transformation initializes (see also Figure 3), which causes temperature to increase. Depending on the specific choice of the heat conductivity, the increase of heat differs:

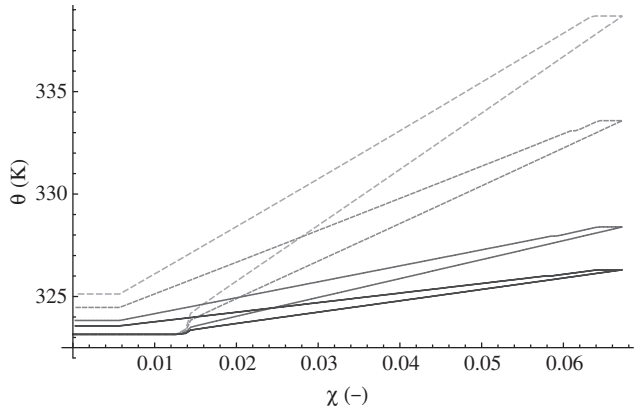

Figure 1 Temperature over strain with varying heat conductivity $\kappa \in \{0.010, 0.015, 0.030, 0.050\}$ GPa/K. Higher temperature evolution is observed at lower values of κ.

it is lowest for κ=0.050 GPa/K and highest for κ=0.010 GPa/K. When the material is unloaded, the elevated temperature remains constant until the phase transformation from the martensitic composition starts, which was established during loading back to austenite. In contrast to the transformation from the thermodynamically stable phase of austenite to martensite when the material was loaded, the back-transformation is endothermic. Thus, during unloading, the material absorbs heat, which causes temperature to decrease. When the back-transformation has finished, temperature remains constant again, but at a higher value than at the beginning. This effect is expected because phase transformations in shape memory alloys are dissipative. Therefore, a part of the mechanically applied power is transformed into heat. This aspect is captured by our material model as demonstrated in Figure 1.

The value for the heat capacity determines the amount of produced heat not only in terms of final values of temperature but also influences shape and size of the hysteresis in the temperature-strain diagram in Figure 1.

Thermomechanical coupling in shape memory alloys takes place bilaterally: due to phase transformations, temperature increases, which in turn has an impact on the evolution of phase transformation. This phenomenon can be observed in Figure 2. Here, the evolution of the austenitic phase over strain is presented. We see that, in the beginning, there is hardly any difference between the cases with varying heat capacity. However, at maximum load, the diagram shows that the amount of remaining austenite is approximately about 2% higher for the simulation with low heat capacity and thus high temperature (gray, dashed curve) compared with the case with large heat capacity (black curve).

Although it may seem at first glance that a difference of approximately 2% in the remaining amount of austenite is of minor importance, the contrary is true as demonstrated in Figure 3. Here, the corresponding stress-strain diagrams are plotted for the simulations with different values for κ. At the very beginning, the

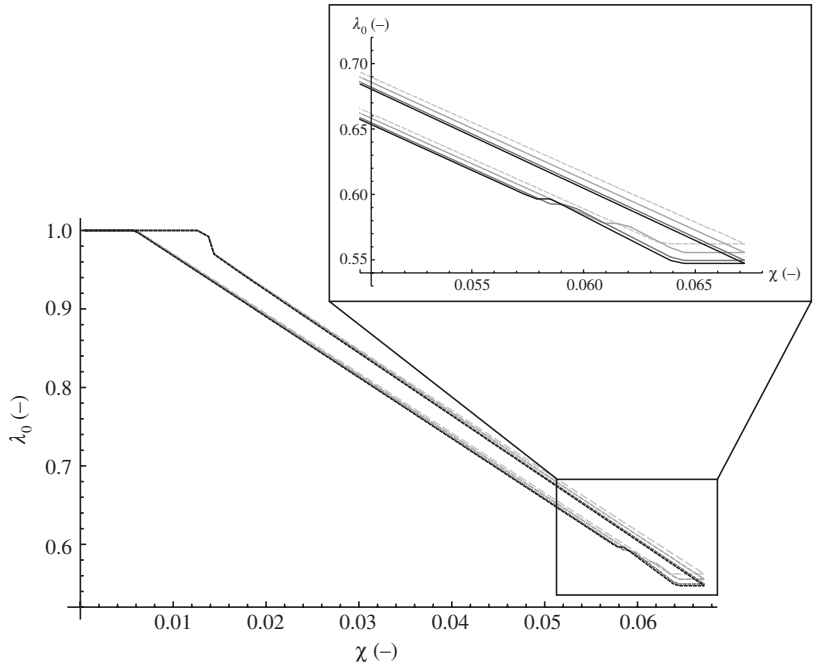

Figure 2 Volume fraction of austenite over strain with varying heat conductivity $\kappa \in \{0.010, 0.015, 0.030, 0.050\}$ GPa/K, including a zoom of the end region.

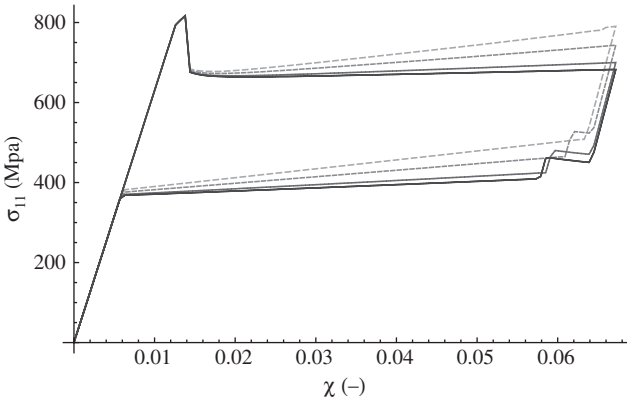

Figure 3 Stress σ_{11} over strain for varying heat conductivity $\kappa \in \{0.010, 0.015, 0.030, 0.050\}$ GPa/K.

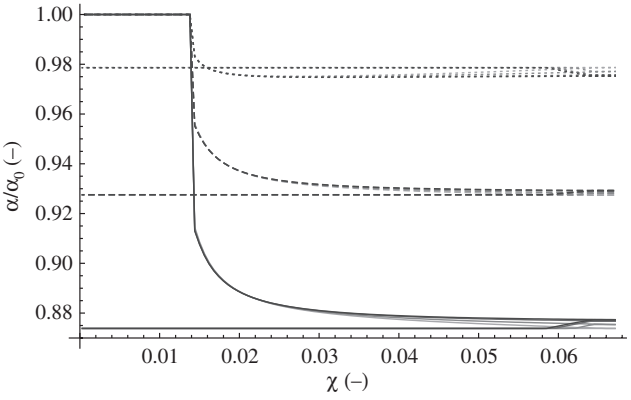

Figure 4 Relative value of the Euler angles over strain for varying heat conductivity $\kappa \in \{0.010, 0.015, 0.030, 0.050\}$ GPa/K, $\boldsymbol{\alpha}_0 = \{2.62596, 1.84057, 5.98139\}$.

material behaves linearly elastic. Then, at a strain of $\chi = 0.0125$, a stress drop takes place when phase transformation starts. This first part of the material reaction is almost independent of the specific choice for the heat conductivity, which is expected because, during that part, the increase in temperature is not yet very pronounced (see Figure 1). After the stress drop, we find the well-known plateau behavior, which is typical during phase transformation in shape memory alloys. Although the load increases further, the difference in the evolution of temperature increases, which stabilizes the austenite as discussed previously (Figure 2). Although the resulting change in the evolution of austenite is not very huge, it is large enough to have a pronounced impact on the resultant stress: whereas stress remains quite constant for a small temperature increase, the stress plateau shows a distinct inclination, which is the more pronounced the higher the temperature is. This aspect corresponds well to experiments [2].

The material model accounts for the polycrystalline martensitic texture by the specific approach for the representative orientation distribution function in terms of evolving Euler angles. The relative value of the Euler angles is presented in Figure 4. Here, all angles start at a relative value of 1. We see that the evolution of the Euler angles differs. For instance, one angle diminishes only by approximately 2%, whereas another angle reduces its value by approximately 12%. This depends on the choice of the initial set of angles. Again, we see some influence when temperature increases with different loading rates. However, here the differences are quite small.

It can be seen that all angles evolve quite drastically when phase transformation initializes. After this initial drop, they remain almost constant. The evolution of the orientation of the average direction of phase transforming grains is dissipative. Thus, the evolution of the relative values for $\boldsymbol{\alpha}$ contributes to the evolution of temperature as well. This explains the nonlinear behavior of the temperature-strain curves in Figure 1 right at the beginning of temperature evolution. This means that we see a similar effect as for the evolution of the volume fraction of austenite: although the difference in the evolution of Euler angles seems to be quite small for different values for κ, these small differences have a measurable impact on temperature evolution.

5 Conclusions

Based on the variational principle of the minimum of the dissipation potential for nonisothermal processes, we derived a thermomechanically coupled material model for polycrystalline shape memory alloys. The application of this variational principle yields more concise governing equations in comparison with the principle of maximum dissipation [19]. To increase numerical efficiency, we adapted a condensed formulation for the distribution orientation functions. Finally, we presented in this paper the first results for the thermomechanically coupled material model on a material point level. Various examples showed that the evolution of temperature as well as the temperature dependence of the stress can be captured very well by our material model. In a future work, we will discuss the model's performance for entire material specimens when it is evaluated within a finite element framework and the artificial assumption of an adiabatic process will not have to be made.

References

[1] Otsuka K, Wayman CM, Eds. *Shape Memory Materials*. Cambridge University Press, 1998. ISBN 0-521-44487-X.

[2] Shaw, JA, Kyriakides, S. *J. Mech. Phys. Solids* 1995, 43, 1243–1281.

[3] Junker P, Makowski J, Hackl K. *Continuum Mech. Thermodyn.* 2013, 1–10.

[4] Hackl K, Schmidt-Baldassari M, Zhang W. *Mater. Sci. Eng. A* 2004, 378, 503–506.

[5] Hackl K, Heinen R. *Continuum Mech. Thermodyn.* 2008, 19, 499.

[6] Junker P, Hackl K. *Comput. Mech.* 2011, 47, 505–517.

[7] Junker P. Simulation of shape memory alloys – material modeling using the principle of maximum dissipation. Ph.D. thesis 2011, urn:nbn:de:hbz:29433862.

[8] Junker P, Hackl K. *Int. J. Structural Changes in Solids* 2009, 3, 49–62.

[9] Auricchio F, Taylor RL. *Comput. Methods Appl. Mech. Eng.* 1997, 143, 175–194.

[10] Bouvet C, Calloch S, Lexcellent C. *Eur. J. Mech. A Solids* 1987, 23, 37–61.

[11] Stein E, Sagar G. *Int. J. Numer. Methods Eng.* 2008, 74, 1–31.

[12] Bartel T, Hackl K. *Proc. Appl. Math. Mech.* 2004, 4, 298–299.

[13] Govindjee S, Miehe C. *Comput. Methods Appl. Mech. Eng.* 2001, 191, 215–238.

[14] Stupkiewicz S, Petryk HJ. *J. Mech. Phys. Solids* 2002, 50, 2303–2331.

[15] Edelen D. *Arch Rat. Mech. Anal.* 1973, 51, 218-227.

[16] Fu S, Huo Y, Müller I. *Acta Mech.* 1993, 99, 1–19.

[17] Wagner MFX, Windl W. *Acta Mater.* 2008, 56, 6232–6245.

[18] Otsuka K, Ren X. *Prog. Mater. Sci.* 2005, 50, 511–678.

[19] Hackl K, Fischer FD. *Proc. R. Soc. A* 2008, 464, 117–132.